



Article

Synthesis of $\text{TiB}_2/\text{TiC}/\text{Al}_2\text{O}_3$ and $\text{ZrB}_2/\text{ZrC}/\text{Al}_2\text{O}_3$ Composites by Low-Exotherm Thermitic Combustion with PTFE Activation

Chun-Liang Yeh *  and Kuan-Ting Liu

Department of Aerospace and Systems Engineering, Feng Chia University, Taichung 40724, Taiwan; m0506707@fcu.edu.tw

* Correspondence: clyeh@fcu.edu.tw; Tel.: +886-4-2451-7250 (ext. 3963)

Abstract: $\text{TiB}_2\text{-TiC-Al}_2\text{O}_3$ and $\text{ZrB}_2\text{-ZrC-Al}_2\text{O}_3$ composites were produced via PTFE (polytetrafluoroethylene)-activated combustion synthesis involving low-exotherm thermites. The reactant stoichiometries were $3\text{TiO}_2 + 4\text{Al} + 0.5\text{B}_4\text{C} + (1 - x)\text{C} + x\text{C}_{\text{PTFE}}$ and $3\text{ZrO}_2 + 4\text{Al} + 0.5\text{B}_4\text{C} + (1 - y)\text{C} + y\text{C}_{\text{PTFE}}$. PTFE played a dual role in promoting the reaction and carburizing reduced Ti and Zr. The threshold amount of PTFE for the TiO_2/Al -based reaction was 2 wt% (i.e., $x = 0.15$) and for the ZrO_2/Al -based reaction was 3 wt% (i.e., $y = 0.25$). The increase in PTFE increased the combustion front velocity and reaction temperature. The TiO_2/Al -based reaction was more exothermic than the ZrO_2/Al -based reaction and exhibited a faster combustion front and a lower activation energy. The $\text{TiB}_2\text{-TiC-Al}_2\text{O}_3$ composite was produced with the minimum amount of PTFE at $x = 0.15$. The formation of $\text{ZrB}_2\text{-ZrC-Al}_2\text{O}_3$ composites required more PTFE at $y = 0.5$ to improve the reduction of ZrO_2 . Both triplex composites displayed mixed microstructures consisting of short-rod borides, fine spherical carbides, and Al_2O_3 agglomerates.

Keywords: triplex ceramic composites; combustion synthesis; PTFE; thermites; activation energy



Citation: Yeh, C.-L.; Liu, K.-T. Synthesis of $\text{TiB}_2/\text{TiC}/\text{Al}_2\text{O}_3$ and $\text{ZrB}_2/\text{ZrC}/\text{Al}_2\text{O}_3$ Composites by Low-Exotherm Thermitic Combustion with PTFE Activation. *J. Compos. Sci.* **2022**, *6*, 111. <https://doi.org/10.3390/jcs6040111>

Academic Editor: Francesco Tornabene

Received: 6 March 2022

Accepted: 6 April 2022

Published: 7 April 2022

Publisher's Note: MDPI stays neutral with regard to jurisdictional claims in published maps and institutional affiliations.



Copyright: © 2022 by the authors. Licensee MDPI, Basel, Switzerland. This article is an open access article distributed under the terms and conditions of the Creative Commons Attribution (CC BY) license (<https://creativecommons.org/licenses/by/4.0/>).

1. Introduction

The development of binary and ternary ceramic matrix composites has gained considerable attention because composite ceramics can overcome the intrinsic brittleness of monolithic ceramics. With a wide range of technological applications, $\text{TiB}_2\text{-TiC}$ and $\text{ZrB}_2\text{-ZrC}$ composites are the most studied boride-carbide composites of the transition metals [1–5]. They possess an exceptional combination of mechanical and physical properties, including high melting points, hardness, flexural strength, thermal shock resistance, chemical stability, and thermal and electrical conductivity, as well as good corrosion and oxidation resistance at high temperatures [4–8]. Additionally, their oxidation resistance, wear resistance, and fracture toughness can be reinforced by Al_2O_3 addition [9–11].

Conventional methods to fabricate multiphase ceramic composites include pressureless sintering, hot pressing, hot isostatic pressing, spark plasma sintering, and mechanochemical reaction [12–17]. As an alternative approach, combustion synthesis or self-propagating high-temperature synthesis (SHS) based on highly exothermic reactions has the advantages of high energy efficiency, a fast reaction rate, simplicity of operation, high-purity products, and in situ formation of composite components [18]. Once the thermite mixtures with strong exothermicity, for example $\text{Fe}_2\text{O}_3/\text{Al}$, MoO_3/Al , and WO_3/Al , are combined with the SHS reaction, thermitic combustion synthesis enhances the degree of reaction sustainability and provides an in situ fabrication route for various Al_2O_3 -reinforced ceramics and intermetallics [19–22]. On the other hand, PTFE (polytetrafluoroethylene or Teflon) has often been employed as a reaction promoter for SHS reactions containing low-exotherm thermites such as $\text{Cr}_2\text{O}_3/\text{Al}$, SiO_2/Al , ZrO_2/Al , and ZrSiO_4/Al [23–25]. Abovyan et al. [24] indicated that the addition of PTFE led to the formation of gas-phase transport species in the $\text{SiO}_2/\text{Al}/\text{C}$ combustion system and promoted the growth of SiC whiskers. The role of

PTFE in transporting the reactant species by metal halides was verified in PTFE-activated combustion synthesis involving aluminothermic reduction of ZrSiO_4 , SiO_2 , and ZrO_2 [25].

The aim of this study was to fabricate triplex ceramic composites of $\text{TiB}_2\text{-TiC-Al}_2\text{O}_3$ and $\text{ZrB}_2\text{-ZrC-Al}_2\text{O}_3$ via low-exotherm thermite combustion synthesis with PTFE activation. Reactant mixtures were formulated using two thermite reagents of TiO_2/Al and ZrO_2/Al , as well as B_4C , carbon black, and PTFE powders. In this study, the effects of PTFE were explored on the initiation of the SHS reaction, variations in combustion velocity and temperature, and evolution of the product phases. The activation energy of the combustion synthesis reaction was deduced from combustion wave kinetics. The composition and microstructure of as-synthesized products were analyzed.

2. Materials and Methods

The starting materials included TiO_2 (Strem Chemicals, Newburyport, MA, USA, <45 μm , 99.5%), ZrO_2 (Alfa Aesar, Ward Hill, MA, USA, <45 μm , 99.5%), Al (Showa Chemical, <45 μm , 99.9%), B_4C (Showa Chemical, Tokyo, Japan, <10 μm , 99.5%), carbon black (Showa Chemical, 20–40 nm, 99%), and PTFE $(-\text{C}_2\text{F}_4)_n-$ (Alfa Aesar, 6–10 μm). Reactant mixtures were prepared based on the stoichiometries of Reactions (R1) and (R2) for the production of $\text{TiB}_2\text{-TiC-Al}_2\text{O}_3$ and $\text{ZrB}_2\text{-ZrC-Al}_2\text{O}_3$ composites, respectively.



where C_{PTFE} signifies carbon supplied from the decomposition of PTFE and is considered as a part of the total carbon balance; that is, PTFE was adopted not only to act as the reaction promoter, but also to participate in carburizing reduced Ti and Zr. The coefficients, x and y , denote the mole content of C_{PTFE} . In R1 and R2, the sources of carbon for the formation of metal carbides include B_4C , carbon black, and PTFE. For the production of metal borides, B_4C is the only source of boron. According to experimental observations in this study, the threshold amount of PTFE for R1 to be initiated was about 2 wt%, which was equivalent to $x = 0.15$, and that for R2 was 3 wt% and $y = 0.25$. To evaluate the effect of the PTFE content on the combustion behavior and product evolution, this study performed x in the range from 0.15 to 0.35 for R1 and y from 0.25 to 0.5 for R2.

The reactant powders were well mixed in a ball mill and then compressed into cylindrical samples measuring 7 mm in diameter, 12 mm in length, and 55% of the relative density. The SHS experiments were conducted in a windowed stainless-steel chamber filled with Ar at 0.3 MPa to ensure an inert environment. The propagation velocity of the combustion wave (V_f) was determined from the time sequence of recorded images. The combustion temperature was measured using a fine-wire thermocouple with an alloy combination of Pt/Pt-13%Rh (Omega Engineering Inc.; Norwalk, CT, USA). The wire diameter was 62.5 μm and the bead size was 125 μm . Details of the experimental setup are reported elsewhere [26]. Constituent phases of the synthesized product were identified by X-ray diffraction (XRD) patterns using an X-ray diffractometer (Bruker D2 Phaser; Billerica, MA, USA) with CuK_α radiation. Scanning electron microscopy (SEM, Hitachi, Tokyo, Japan) analysis was performed with energy-dispersive spectroscopy (EDS, Hitachi, Tokyo, Japan) to examine the microstructure and elemental composition on the fracture surface of the final product.

It has been empirically recognized by Merzhanov [27] that the adiabatic temperature (T_{ad}) of a solid-state combustion reaction higher than 1800 K is a criterion for establishing a self-sustaining combustion process. T_{ad} was calculated for PTFE-free R1 and R2 reactions via an energy balance equation [26] with thermochemical data taken from [28].

3. Results and Discussion

3.1. Thermodynamic Analysis

The aluminothermic reduction of metal oxides (TiO_2 and ZrO_2) is considered as the initiating step in R1 and R2 but the solid-state combustion of R1 and R2 cannot start off without the activation of PTFE. This could be due to the weak reaction exothermicity or the high kinetic barrier of the initiation reaction. As shown in Figure 1, the calculated values of the reaction enthalpy (ΔH_r) and T_{ad} are relatively low for the aluminothermic reduction of TiO_2 and ZrO_2 , especially in the case of $3\text{ZrO}_2 + 4\text{Al}$. Unlike most of the thermites with T_{ad} exceeding 3500 K [29], TiO_2/Al and ZrO_2/Al mixtures are low-exotherm thermites. Figure 1 also shows significant increases in ΔH_r and T_{ad} for R1 and R2, since their products, namely transition metal boride (TiB_2 and ZrB_2) and carbide (TiC and ZrC), are high-exotherm compounds. Moreover, TiO_2/Al -based R1 is more exothermic than ZrO_2/Al -based R2. Even although R1 and R2 have T_{ad} values of 2665 K and 2080 K, respectively, it was found that their initiation was infeasible without PTFE addition. As a reaction promoter, PTFE is able to facilitate solid-phase diffusion by means of the gas-phase transport agent to overcome the kinetic limitation and assist the synthesis reaction to proceed [30].

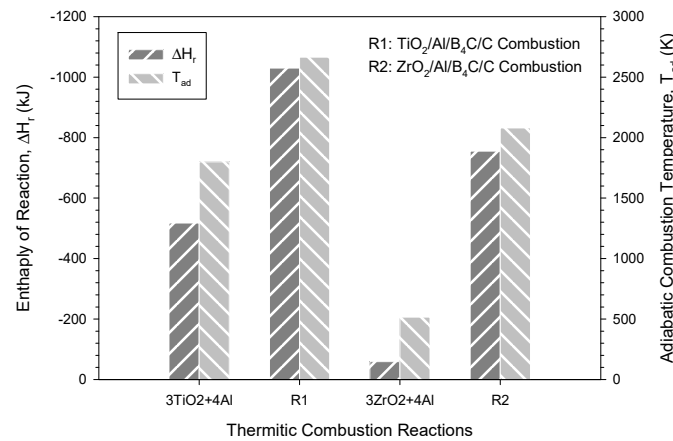


Figure 1. Enthalpies of reaction (ΔH_r) and adiabatic combustion temperatures (T_{ad}) of thermite combustion reactions.

3.2. Self-Propagating Combustion Kinetics

With the addition of PTFE at $x = 0.15$ in R1 and $y = 0.35$ in R2, Figure 2a,b represent typical SHS processes, which illustrate that upon ignition, self-sustaining combustion is achieved and a distinct combustion wave traverses the powder compact. Because of the generation of gaseous species associated with PTFE, gas discharged from the powder compacted during combustion wave progression, leading to the formation of pores and cracks in the burned sample and an elongated final product.

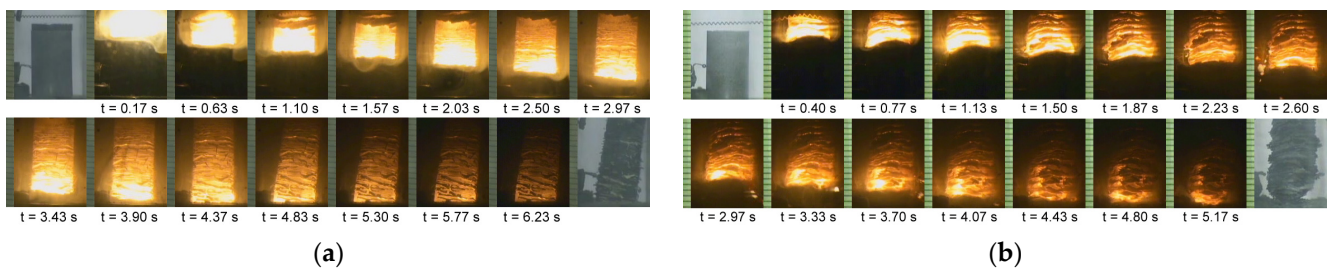


Figure 2. Time sequences of self-sustaining combustion images recorded from PTFE-activated thermite combustion: (a) TiO_2/Al -based reaction R1 with $x = 0.15$; (b) ZrO_2/Al -based reaction R2 with $y = 0.35$.

The effect of the PTFE content on the flame-front propagation velocity of R1 and R2 is presented in Figure 3a. The increase in PTFE from $x = 0.15$ to 0.35 was found to accelerate the combustion wave of R1 from $V_f = 2.68$ to 4.17 mm/s. A slower combustion wave was observed for R2, most likely due to its weaker reaction exothermicity, with the wave speeds ranging from 1.74 to 2.95 mm/s for the PTFE content from $y = 0.35$ to 0.5 . It has been proposed that gas-phase transport agents in the form of metal fluorides can effectively improve the solid-phase diffusion, which is critical for solid-state combustion to proceed in a self-sustaining manner [30]. Regarding metal fluorides, TiF_3 could be produced in R1 from the interaction of C_2F_4 with TiO_2 and ZrF_4 in R2 from C_2F_4 reacting with ZrO_2 [25,31].

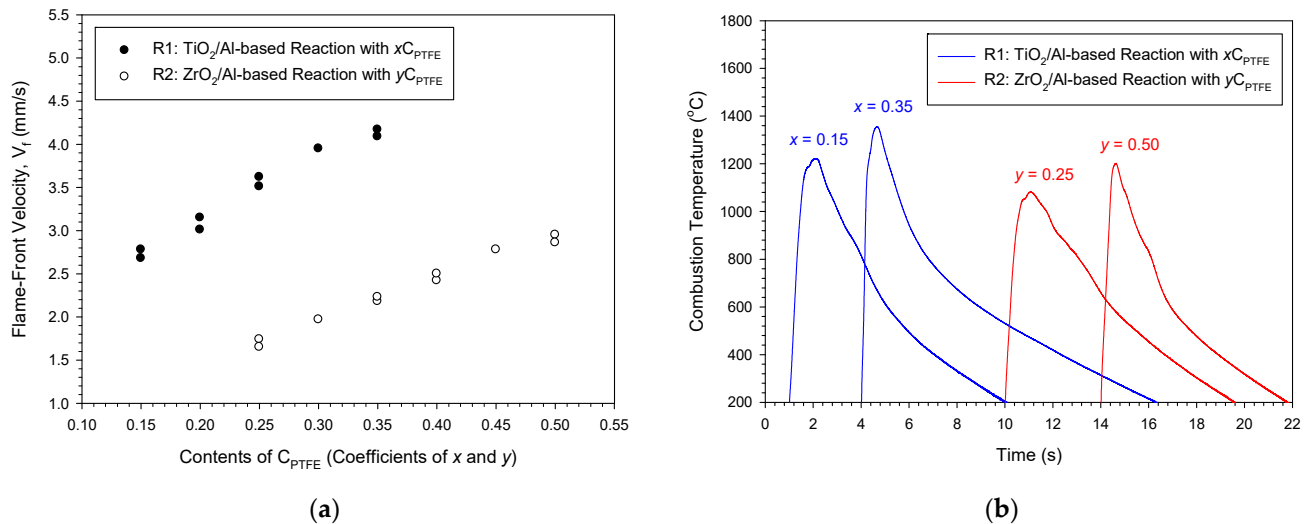


Figure 3. Effects of PTFE content on (a) combustion wave velocities and (b) combustion temperatures of TiO_2/Al - and ZrO_2/Al -based thermite combustion reactions R1 and R2.

Figure 3b depicts typical combustion temperature profiles of R1 and R2. The contours feature an abrupt rise to their peak points, followed almost immediately by a substantial decline due to heat losses to the surroundings. The sharp surge signifies the fast arrival of the combustion wave and the peak value represents the combustion front temperature (T_c). An increase in T_c with PTFE content was noticed for both R1 and R2. As indicated in Figure 3b, T_c is about 1222 $^{\circ}C$ for R1 with $x = 0.15$ and reaches 1356 $^{\circ}C$ as the PTFE content increases to $x = 0.35$. Due to the weaker reaction exothermicity, lower T_c values of about 1082 and 1202 $^{\circ}C$ were measured for R2 with PTFE at $y = 0.35$ and 0.50 , respectively. The increase in T_c with increasing PTFE content meant a thermal assistance from PTFE, because gas-phase metal fluorides are highly exothermic intermediates [32]. For example, the formation enthalpies of TiF_3 and ZrF_4 are -1188.7 and -1673.6 kJ/mol, respectively [28]. As stated by Merzhanov [27], even a small amount of gaseous transport species can make a significant impact on the SHS process, leading to pronounced changes in the combustion propagation speed, reaction temperature, elongation of the product, and phase transformation from reactants to products.

The correlation of the combustion wave velocity with the reaction temperature was applied to determine the activation energy (E_a) of the solid-state combustion reaction from the slope of a best-fitted linear line in the plot of $\ln(V_f/T_c)^2$ versus $1/T_c$ [33]. As presented in Figure 4, the values of E_a equal to 102.3 and 123.9 kJ/mol were deduced for R1 and R2, respectively. A lower E_a suggests that R1 is more favorable in the kinetic aspect. Thermally, R1 is also more energetic. This explained why the threshold amount of PTFE required to trigger the SHS process was lesser for R1 than R2.

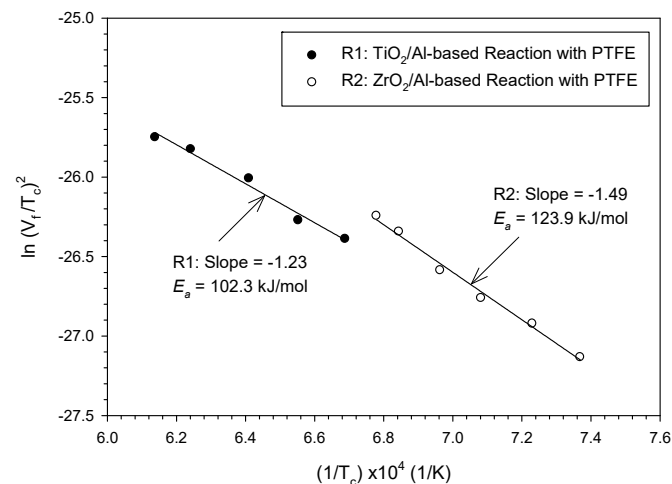


Figure 4. Activation energies (E_a) of PTFE-activated TiO₂/Al- and ZrO₂/Al-based thermitic combustion reactions deduced from the correlation of the combustion front velocity (V_f) with temperature (T_c).

The role of PTFE in activating the reaction is two-fold: it first has to overcome the kinetic limitation due mostly to the insufficient reactivity caused by the presence of diffusion barriers, and secondly it has to enhance the degree of reaction exothermicity. Once gas-phase metal fluorides, TiF₃ and ZrF₄, were generated, they diffused to B₄C or carbon particles and brought about condensation of Ti and Zr on the solid particles [31,34]. The deposition of metallic compounds on B₄C and carbon facilitated their interactions to produce high-exotherm metal borides and carbides; that is, the reaction assisted by the gas-phase transport mechanism is benefited in both kinetical and thermal aspects. As soon as the initiation step was triggered, aluminothermic reduction of TiO₂ and ZrO₂ took place and then reduced Ti and Zr, which reacted with B₄C and carbon.

The discharge of volatile metal fluorides into the air might cause water and soil pollution. This results in a number of problems in the environment, including decreased plant growth and crop yield. Harmful effects of fluoride on the health problems of animals have also been reported [35]. In this study, the exhaust gas was treated through a filter containing absorbent particles of synthetic aluminum oxide, which acted as the fluoride removal media [36].

3.3. Phase Composition and Microstructure of Synthesized Products

The products of SHS were crushed and ground into powders for the XRD analysis by using a porcelain mortar and pestle. The XRD patterns of SHS-derived products from R1 with PTFE values of $x = 0.15$ and 0.35 are presented in Figure 5a,b, respectively. Both samples produced triplex composites composed of TiB₂, TiC, and Al₂O₃. The crystal structures and powder diffraction data for TiB₂ refer to JCPDS (Joint Committee on Powder Diffraction Standards) card number 85-2083, TiC to JCPDS 89-3828, and Al₂O₃ to JCPDS 88-0826 [37]. No unreacted reagents or impurities were detected, even for the sample with the threshold amount of PTFE of $x = 0.15$; that is, the complete conversion from the reactants to products was achieved by R1 under PTFE activation.

Figure 6a,b contains a representation of the XRD patterns, which were collected for the zirconium-containing samples. Three target phases, ZrB₂ (JCPDS 89-3930), ZrC (JCPDS 89-4054), and Al₂O₃, were identified along with ZrO₂. The existence of ZrO₂ indicates incomplete aluminothermic reduction. It was found that the increase in PTFE from $y = 0.35$ (the threshold amount) to $y = 0.5$ decreased ZrO₂ considerably. According to Lee et al. [38], PTFE is able to remove the oxide shell on the surface of Al particles and to enhance the reactivity of Al. As a consequence, the reduction of ZrO₂ by Al was improved and the amount of ZrO₂ left in the final product was trivial, as shown in Figure 6b.

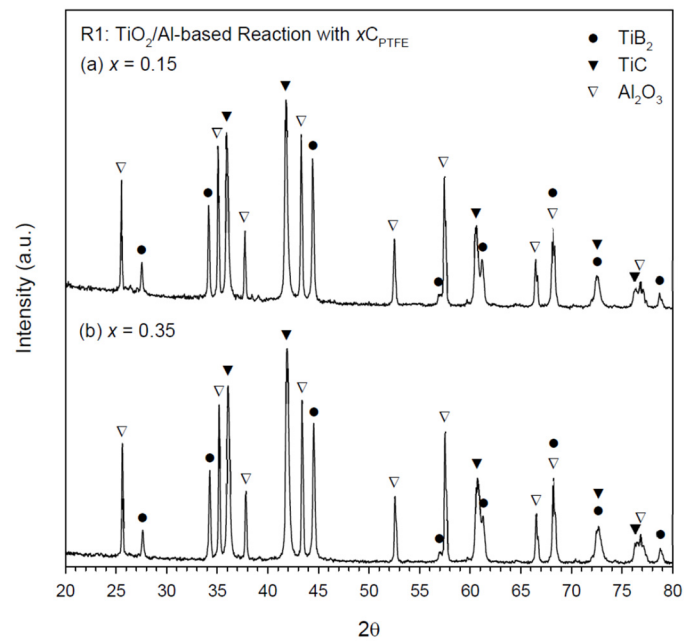


Figure 5. XRD patterns of $\text{TiB}_2/\text{TiC}/\text{Al}_2\text{O}_3$ composites synthesized from PTFE-activated thermite combustion reaction R1 with (a) $x = 0.15$ and (b) $x = 0.35$.

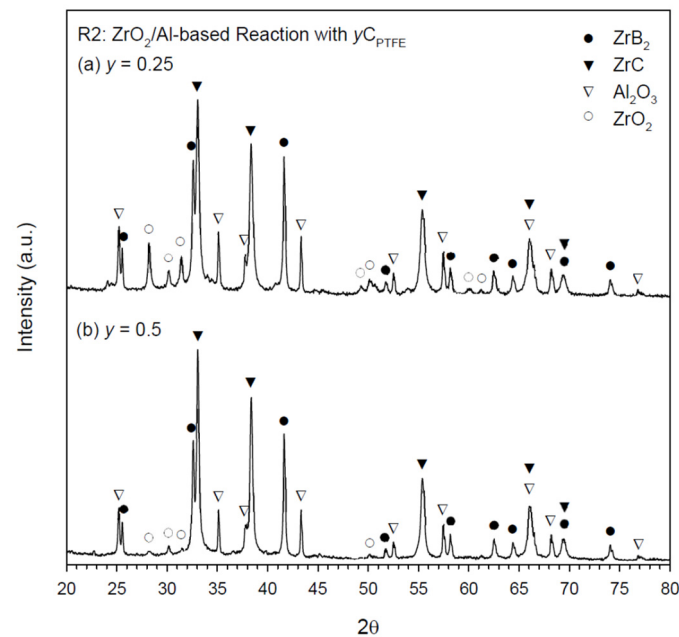


Figure 6. XRD patterns of $\text{ZrB}_2/\text{ZrC}/\text{Al}_2\text{O}_3$ composites synthesized from PTFE-activated thermite combustion reaction R2 with (a) $y = 0.25$ and (b) $y = 0.5$.

Figures 7 and 8 present SEM images and EDS spectra of the fracture surfaces of the products synthesized from R1 with $x = 0.25$ and R2 with $y = 0.5$, respectively. As illustrated in Figure 7, the composite is composed of TiB_2 , TiC , and Al_2O_3 with different morphologies, including short rods of TiB_2 (with length of 3–4 μm), small spheres of TiC (about 1–2 μm), and agglomerated grains of Al_2O_3 (about 5–7 μm). Because of the formation of gas-phase species during combustion, the discharge of gases created pores and cracks and caused delamination and elongation of the product. Therefore, the final products were porous, constituent grains were loosely bound, and composite powders were easy to obtain. The EDS spectrum of Figure 7 reveals the detection of all five elements from the SEM image.

The quantitative elemental percentages are in reasonable agreement with the product composition of $TiB_2 + 2TiC + 2Al_2O_3$ in R1.

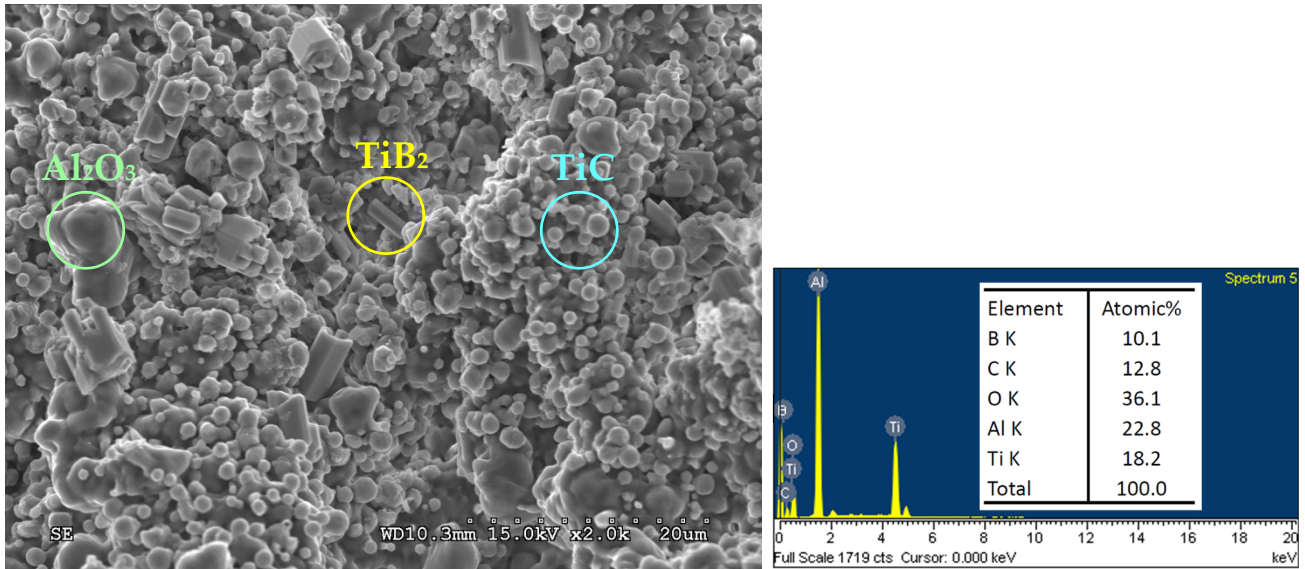


Figure 7. SEM micrograph and EDS spectrum of $TiB_2/TiC/Al_2O_3$ composite synthesized from PTFE-activated thermite reaction R1 with $x = 0.25$.

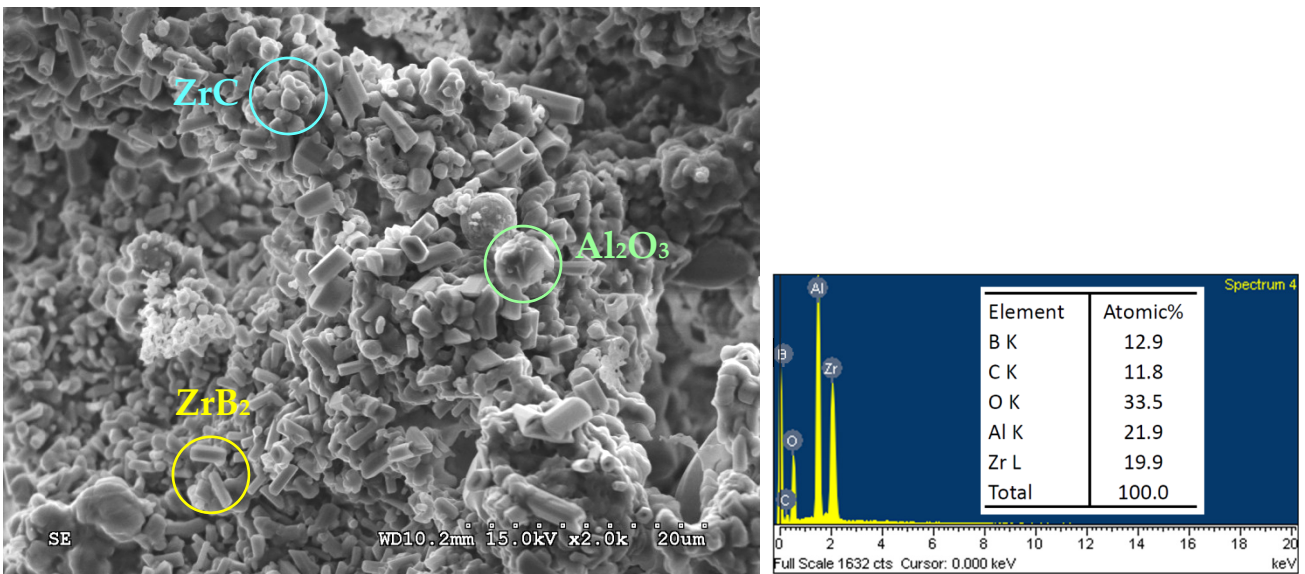


Figure 8. SEM micrograph and EDS spectrum of $ZrB_2/ZrC/Al_2O_3$ composite synthesized from PTFE-activated thermite reaction R2 with $y = 0.5$.

The SEM image in Figure 8 shows that the microstructure of the $ZrB_2-ZrC-Al_2O_3$ composite of R2 is similar to that of the $TiB_2-TiC-Al_2O_3$ composite of R1. Short-rod ZrB_2 , fine spherical ZrC , and granular Al_2O_3 can be clearly observed in Figure 8. Additionally, the EDS analysis detected all five elements and provided an elemental ratio. The atomic percentages reported in Figure 8 are close to the composition of $ZrB_2 + 2ZrC + 2Al_2O_3$.

The grain sizes of SHS-derived products were reduced with different methods, such as by decreasing the combustion temperature; introducing modifiers; fast cooling of the product after the synthesis; and applying compaction, extrusion, shock waves, or ultrasonic waves in the process [39,40]. Hot pressing is typically applied for pressing and sintering of SHS-derived ceramic powders to obtain bulk ceramics in dense form and with a ho-

mogeneous microstructure [41]. Spark plasma sintering (SPS) is another method used to consolidate SHS-produced powders [42]. The HP approach is characterized by relatively long processing times (typically of the order of hours) because of the low heating rates. On the contrary, the SPS method involves a pulsed-current process in which the powder samples are loaded in an electrically conducting dye to accelerate the heating process and then sintered under uniaxial pressure.

4. Conclusions

Two triplex composites $\text{TiB}_2\text{-TiC-Al}_2\text{O}_3$ and $\text{ZrB}_2\text{-ZrC-Al}_2\text{O}_3$ were produced via PTFE-activated combustion synthesis involving the aluminothermic reduction of TiO_2 and ZrO_2 . Reactant mixtures were prepared based on $3\text{TiO}_2 + 4\text{Al} + 0.5\text{B}_4\text{C} + (1 - x)\text{C} + x\text{C}_{\text{PTFE}}$ and $3\text{ZrO}_2 + 4\text{Al} + 0.5\text{B}_4\text{C} + (1 - y)\text{C} + y\text{C}_{\text{PTFE}}$. Both reaction systems required the addition of PTFE to assist their initiation and the establishment of self-sustaining combustion. PTFE played a dual role in promoting the reaction and carburizing Ti and Zr. Experimental evidence indicated that the threshold amount of PTFE for the TiO_2/Al -based reaction was 2 wt% (i.e., $x = 0.15$) and for the ZrO_2/Al -based reaction was 3 wt% (i.e., $y = 0.25$). The increase in PTFE content accelerated the combustion wave and elevated the combustion temperature. The TiO_2/Al -based reaction was more exothermic than the ZrO_2/Al -based reaction and exhibited a faster combustion front. Based on the correlation of the combustion front velocity with temperature, E_a values of 102.3 and 123.9 kJ/mol were deduced for PTFE-activated TiO_2/Al - and ZrO_2/Al -based combustion reactions, respectively.

The XRD pattern confirmed that the $\text{TiB}_2\text{-TiC-Al}_2\text{O}_3$ composite was well produced from TiO_2/Al -based combustion with the minimum amount of PTFE added at $x = 0.15$. SEM graphs displayed a mixed microstructure consisting of TiB_2 in the form of short rods, TiC of micro-sized spheres, and Al_2O_3 agglomerates. However, the incomplete reduction of ZrO_2 was observed in the synthesis of $\text{ZrB}_2\text{-ZrC-Al}_2\text{O}_3$ composites. The reduction of ZrO_2 by Al was improved by increasing the PTFE, and the final product containing a negligible amount of ZrO_2 was obtained from the sample with PTFE of $y = 0.5$.

Author Contributions: Conceptualization, C.-L.Y.; methodology, C.-L.Y. and K.-T.L.; validation, C.-L.Y. and K.-T.L.; formal analysis, C.-L.Y. and K.-T.L.; investigation, C.-L.Y. and K.-T.L.; resources, C.-L.Y.; data curation, C.-L.Y. and K.-T.L.; writing—original draft preparation, C.-L.Y. and K.-T.L.; writing—review and editing, C.-L.Y.; supervision, C.-L.Y.; project administration, C.-L.Y.; funding acquisition, C.-L.Y. All authors have read and agreed to the published version of the manuscript.

Funding: This research work was funded by the Ministry of Science and Technology of Taiwan under the grant of MOST 110-2221-E-035-042-MY2.

Institutional Review Board Statement: Not applicable.

Informed Consent Statement: Not applicable.

Data Availability Statement: Data presented in this study are available in the article.

Conflicts of Interest: The authors declare no conflict of interest.

References

1. Alsawat, M.; Altalhi, T.; Alotaibi, N.F.; Zaki, Z.I. Titanium carbide—Titanium boride composites by self propagating high temperature synthesis approach: Influence of zirconia additives on the mechanical properties. *Results Phys.* **2019**, *13*, 102292. [[CrossRef](#)]
2. Tsuchida, T.; Yamamoto, S. Mechanical activation assisted self-propagating high-temperature synthesis of ZrC and ZrB_2 in air from Zr/B/C powder mixtures. *J. Eur. Ceram. Soc.* **2004**, *24*, 45–51. [[CrossRef](#)]
3. Zhang, M.; Huo, Y.; Huang, M.; Fang, Y.; Zou, B. In situ synthesis and formation mechanism of ZrC and ZrB_2 by combustion synthesis from the Co-Zr- B_4C system. *J. Asian Ceram. Soc.* **2015**, *3*, 271–278. [[CrossRef](#)]
4. Vallauri, D.; Atías Adrián, I.C.; Chrysanthou, A. TiC– TiB_2 composites: A review of phase relationships, processing and properties. *J. Eur. Ceram. Soc.* **2008**, *28*, 1697–1713. [[CrossRef](#)]
5. Xu, Z.; Zhao, K.; Li, F.; Hou, Y.; Tang, Y. The oxidation behavior of $\text{ZrB}_2\text{-ZrC}$ composite nanofibers fabricated by electrospinning and carbothermal reduction. *Ceram. Int.* **2020**, *46*, 10409–10415. [[CrossRef](#)]

6. Wang, Y.; Yao, M.; Hu, Z.; Li, H.; Ouyang, J.H.; Chen, L.; Huo, S.; Zhou, Y. Microstructure and mechanical properties of TiB₂-40 wt% TiC composites: Effects of adding a low-temperature hold prior to sintering at high temperatures. *Ceram. Int.* **2018**, *44*, 23297–23300. [[CrossRef](#)]
7. Neuman, E.W.; Hilmas, G.E.; Fahrenholtz, W.G. Ultra-high temperature mechanical properties of a zirconium diboride–zirconium carbide ceramic. *J. Am. Ceram. Soc.* **2016**, *99*, 597–603. [[CrossRef](#)]
8. Guo, S.Q.; Kagawa, Y.; Nishimura, T.; Chung, D.; Yang, J.M. Mechanical and physical behavior of spark plasma sintered ZrC–ZrB₂–SiC composites. *J. Eur. Ceram. Soc.* **2008**, *28*, 1279–1285. [[CrossRef](#)]
9. Xu, J.; Zou, B.; Tao, S.; Zhang, M.; Cao, X. Fabrication and properties of Al₂O₃–TiB₂–TiC/Al metal matrix composite coatings by atmospheric plasma spraying of SHS powders. *J. Alloys Compd.* **2016**, *672*, 251–259. [[CrossRef](#)]
10. Li, Z.; Wei, M.; Xiao, K.; Bai, Z.; Xue, W.; Dong, C.; Wei, D.; Li, X. Microhardness and wear resistance of Al₂O₃–TiB₂–TiC ceramic coatings on carbon steel fabricated by laser cladding. *Ceram. Int.* **2019**, *45*, 115–121. [[CrossRef](#)]
11. Xiao, G.Q.; Fu, Y.L.; Zhang, Z.W.; Hou, A.D. Mechanism and microstructural evolution of combustion synthesis of ZrB₂–Al₂O₃ composite powders. *Ceram. Int.* **2015**, *41*, 5790–5797. [[CrossRef](#)]
12. Xu, C. Preparation and performance of an advanced multiphase composite ceramic material. *J. Eur. Ceram. Soc.* **2005**, *25*, 605–611. [[CrossRef](#)]
13. Kim, D.K.; Kriven, W.M. Processing and characterization of multiphase ceramic composites part II: Triplex composites with a wide sintering temperature range. *J. Am. Ceram. Soc.* **2008**, *91*, 793–798. [[CrossRef](#)]
14. Aydin, H.; Elmusa, B. Fabrication and characterization of Al₂O₃–TiB₂ nanocomposite powder by mechanochemical processing. *J. Aust. Ceram. Soc.* **2021**, *57*, 731–741. [[CrossRef](#)]
15. Popov, O.; Chornobuk, S.; Vishnyakov, V. Structure formation of TiB₂–TiC–B₄C–C hetero-modulus ceramics via reaction hot pressing. *Int. J. Refract. Met. Hard Mater.* **2017**, *64*, 106–112. [[CrossRef](#)]
16. Venkatachalam, V.; Blem, S.; Gülhan, A.; Binner, J. Thermal qualification of the UHTCMCs produced using RF-CVI technique with VMK facility at DLR. *J. Compos. Sci.* **2022**, *6*, 24. [[CrossRef](#)]
17. Arai, Y.; Marumo, T.; Inoue, R. Use of Zr–Ti alloy melt infiltration for fabricating carbon-fiber-reinforced ultrahigh-temperature ceramic matrix composites. *J. Compos. Sci.* **2021**, *5*, 186. [[CrossRef](#)]
18. Levashov, E.A.; Mukasyan, A.S.; Rogachev, A.S.; Shtansky, D.V. Self-propagating high-temperature synthesis of advanced materials and coatings. *Int. Mater. Rev.* **2017**, *62*, 203–239. [[CrossRef](#)]
19. Yeh, C.L.; Chen, K.T. Fabrication of FeSi/α-FeSi₂—Based composites by metallothermally assisted combustion synthesis. *J. Aust. Ceram. Soc.* **2021**, *57*, 1415–1424. [[CrossRef](#)]
20. Kirakosyan, H.; Nazaretyan, K.; Aydinyan, S.; Kharatyan, S. The mechanism of joint reduction of MoO₃ and CuO by combined Mg/C reducer at high heating rates. *J. Compos. Sci.* **2021**, *5*, 318. [[CrossRef](#)]
21. Myint Maung, S.T.; Chanadee, T.; Niyomwas, S. Two reactant systems for self-propagating high-temperature synthesis of tungsten silicide. *J. Aust. Ceram. Soc.* **2019**, *55*, 873–882. [[CrossRef](#)]
22. Gibot, P.; Puel, E. Study on indium (III) oxide/aluminum thermite energetic composites. *J. Compos. Sci.* **2021**, *5*, 166. [[CrossRef](#)]
23. Yeh, C.L.; Liou, G.T. A novel route for synthesis of alumina–chromium carbide composites from PTFE-activated Cr₂O₃/Al/C combustion. *Ceram. Int.* **2018**, *44*, 19486–19491. [[CrossRef](#)]
24. Abovyan, L.S.; Nersisyan, H.H.; Kharatyan, S.L.; Orrù, R.; Saiu, R.; Cao, G.; Zedda, D. Synthesis of alumina–silicon carbide composites by chemically activated self-propagating reactions. *Ceram. Int.* **2001**, *27*, 163–169. [[CrossRef](#)]
25. Yeh, C.L.; Wang, Y.H. Preparation of ZrB₂–SiC–Al₂O₃ composites by SHS method with aluminothermic reduction. *Ceram. Int.* **2021**, *47*, 11202–11208. [[CrossRef](#)]
26. Yeh, C.-L.; Chen, K.-T.; Shieh, T.-H. Effects of Fe/Si stoichiometry on formation of Fe₃Si/FeSi–Al₂O₃ composites by aluminothermic combustion synthesis. *Metals* **2021**, *11*, 1709. [[CrossRef](#)]
27. Merzhanov, A.G. Combustion processes that synthesize materials. *J. Mater. Process. Technol.* **1996**, *56*, 222–241. [[CrossRef](#)]
28. Binnewies, M.; Milke, E. *Thermochemical Data of Elements and Compounds*; Wiley-VCH Verlag GmbH: Weinheim, Germany, 2002.
29. Wang, L.L.; Munir, Z.A.; Maximov, Y.M. Thermite reactions: Their utilization in the synthesis and processing of materials. *J. Mater. Sci.* **1993**, *28*, 3693–3708. [[CrossRef](#)]
30. Kim, T.; Wooldridge, M.S. Catalytically assisted self-propagating high-temperature synthesis of tantalum carbide powders. *J. Am. Ceram. Soc.* **2001**, *84*, 976–982. [[CrossRef](#)]
31. Licheri, R.; Orrù, R.; Cao, G. Chemically-activated combustion synthesis of TiC–Ti composites. *Mater. Sci. Eng. A* **2004**, *367*, 185–197. [[CrossRef](#)]
32. Yang, K.; Yang, Y.; Lin, Z.M.; Li, J.T.; Du, J.S. Mechanical-activation-assisted combustion synthesis of SiC powders with polytetrafluoroethylene as promoter. *Mater. Res. Bull.* **2007**, *42*, 1625–1632. [[CrossRef](#)]
33. Varma, A.; Rogachev, A.S.; Mukasyan, A.S.; Hwang, S. Combustion synthesis of advanced materials: Principals and applications. *Adv. Chem. Eng.* **1998**, *24*, 79–225.
34. Oppermann, H. The role of halogens, halogenides, oxide halogenides and their complexes in chemical transport reactions. *Solid State Ionics* **1990**, *39*, 17–25. [[CrossRef](#)]
35. Chen, J.; Qian, H.; Wu, H.; Gao, Y.; Li, X. Assessment of arsenic and fluoride pollution in groundwater in Dawukou area, Northwest China, and the associated health risk for inhabitants. *Environ. Earth Sci.* **2017**, *76*, 314. [[CrossRef](#)]

36. Ghorai, S.; Pant, K.K. Equilibrium, kinetics and breakthrough studies for adsorption of fluoride on activated alumina. *Sep. Purif. Technol.* **2005**, *42*, 265–271. [[CrossRef](#)]
37. Gates-Rector, S.; Blanton, T. The powder diffraction file: A quality materials characterization database. *Powder Diffr.* **2019**, *34*, 352–360. [[CrossRef](#)]
38. Lee, T.-H.; Nersisyan, H.H.; Jeong, H.-G.; Lee, K.-H.; Noh, J.-S.; Lee, J.-H. Efficient synthesis route to quasi-aligned and high-aspect-ratio aluminum nitride micro- and nanostructures. *Chem. Eng. J.* **2011**, *174*, 461–466. [[CrossRef](#)]
39. Merzhanov, G.; Rogachev, A.S. Structural macrokinetics of SHS processes. *Pure Appl. Chem.* **1992**, *64*, 941–953.
40. Mishra, S.K.; Das, S.K.; Sherbacov, V. Fabrication of Al₂O₃–ZrB₂ in situ composite by SHS dynamic compaction: A novel approach. *Compos. Sci. Technol.* **2007**, *67*, 2447–2453. [[CrossRef](#)]
41. Lee, J.H.; Ko, S.K.; Won, C.W. Sintering behavior of Al₂O₃–TiC composite powder prepared by SHS process. *Mater. Res. Bull.* **2001**, *36*, 989–996. [[CrossRef](#)]
42. Licheri, R.; Orrù, R.; Musa, C.; Cao, G. Combination of SHS and SPS techniques for fabrication of fully dense ZrB₂–ZrC–SiC composites. *Mater. Lett.* **2008**, *62*, 432–435. [[CrossRef](#)]